Gear Collision Reduction of Geared In-wheel-motor by Effective Use of Load-side Encoder

Seigo Wakui, Tomoki Emmei, Hiroshi Fujimoto, Yoichi Hori
The University of Tokyo
5-1-5, Kashiwanoha, Kashiwa, Chiba, 277-8561, Japan
Email : wakui.seigo18@ae.k.u-tokyo.ac.jp

***Abstract*—Requirement of large motor torque with limited mounting space for In-wheel-motors (IWMs) expects a geared drivetrain, but the vibration and noise caused by gear collision deteriorates ride comfort. In our previous study, our research group proposed to apply joint torque control using motor-side encoders and additional load-side encoders to geared IWMs and the effectiveness is validated. However, in point of space and costs, the effect of mounting load-side encoders should be investigated carefully. In this paper, joint torque control using both motor-side and load-side encoders is compared with joint torque control using only motor-side encoders. Simulations and experiments demonstrate that load-side encoders make it possible to design controller without vehicle parameters and to reduce the impact of collision sufficiently.**

***Index Terms*—In-wheel-motor, two-inertia system, backlash, joint torque control, load-side encoder.**

I. INTRODUCTION

Electric vehicles (EVs) are gathering considerable attentions due to a greater deal of the concern for environmental problems. However, their short mileage per charge is recognized as a problem and in-motion wireless power transfer system is studied [1]. Advantages of EVs are not only their environmental benefits but also their high motion performance [2], [3]. Response speed of motors is hundreds times faster than that of gasolines.

EVs' drivetrain can be classified into on-board motors and in-wheel-motors (IWMs) according to the arrangement of motors. The performance of on-board motors is limited by low frequent resonance of long drive shafts, while that of IWMs can be enhanced thanks to the absence of drive shafts [4]. This is indicated in the successful studies on various traction control methods [5]. In these studies, direct drive IWMs (DD-IWMs), which has no gears, are used because gear collision make it difficult to control a vehicle. However, the required specifications for IWMs are severe (e.g. large maximum torque, limited mounting space, and low cost etc.). Therefore, geared IWMs (G-IWMs) are desirable to address these requirements [6] and a collision reduction method for G-IWMs should be proposed.

The vibration caused by gear collision has been studied for decades [7], [8]. Most of the studies assume the industrial robot applications and the number of studies which propose vibration suppression methods for EVs is limited [9]. Our research group proposed to apply joint torque control for two-inertia system to G-IWMs in EVs [10]. In [10], a G-IWM is modeled as two-inertia system shown in Fig. 1, where a motor and a load are connected with rigid gears or shafts. Various joint torque control methods for two-inertia system were studied and require different sensor configurations (e.g. only motor-side encoders in [11], joint torque sensors in [12]). With only motor-side encoders and joint torque sensors, it is difficult to suppress the vibration due to the unknown load-side information. Therefore, in recent years, joint torque control using load-side encoders has been studied [13], [14]. Our research group developed G-IWMs with both motor-side and load-side encoders and proposed to apply joint torque control using both motor-side and load-side encoders to G-IWMs for gear collision reduction [10]. However, mounting additional load-side encoders is not desirable in point of space and costs and the effect of it should be investigated carefully.

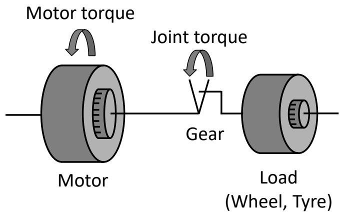

Fig. 1. Two-inertia system.

In this paper, joint torque control using load-side encoders is compared with that of joint torque control using only motor-side encoders and advantages of using load-side encoders are revealed. Load-side information make it possible to control joint torque without vehicle parameters and to reduce the impact of gear collision.

II. EXPERIMENTAL SETUP

A. Experimental Vehicle

The FPEV-4 Sawyer shown in Fig. 2 is used as the experimental vehicle. Our research group developed it based on the commercial EV "i-MiEV" produced by Mitsubishi Motors Corporation. The two rear motors shown in Fig. 3 are G-IWMs with both motor-side and load-side encoders.

B. G-IWM Unit with Both Motor-side and Load-side Encoders

Fig. 4 shows the cross section of our developed G-IWM unit. Encoders are manufactured by Nikon corporation and their resolution is 20 bit. The load-side encoder is equipped

978-1-7281-4878-6/19/$31.00 ©2019 IEEE

Fig. 2. Experimental vehicle FPEV4-Sawyer.

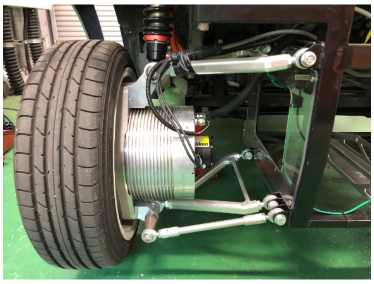

Fig. 3. G-IWM unit with motor-side and load-side encoders.

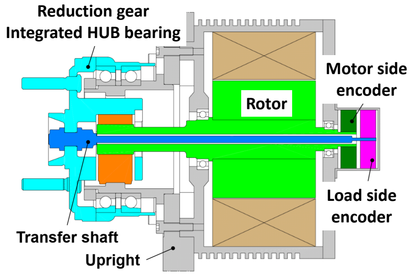

Fig. 4. Cross section of the G-IWM unit.

on the motor side, connected with the load side through the transfer shaft. Mechanical resonance frequency of the shaft is sufficiently high because the shaft rigidity is high and the inertia of the load-side encoder is very small. Therefore, the shaft does not affect the controllability of G-IWMs.

C. IWM model

A G-IWM is modeled as two-inertia system. There are some ways to model backlash [8]. In two-inertia system, backlash can be modeled as memoryless deadzone function. The equations of rotational motion are expressed as (1a)-(1c) :

$$J_m \dot{\omega}_m = T_m - T_s, \tag{1a}$$
$$J_l \dot{\omega}_l = gT_s - rF_d, \tag{1b}$$
$$T_s = K \cdot \mathrm{bl}(\Delta\theta). \tag{1c}$$

The definition of parameters is shown in TABLE I. $\mathrm{bl}(\Delta\theta)$, which is expressed as (2) and shown in Fig. 5, means deadzone function.

$$\mathrm{bl}(\Delta\theta) = \begin{cases} \Delta\theta + \frac{L}{2} & \left(\Delta\theta < -\frac{L}{2}\right), \\ 0 & \left(-\frac{L}{2} \leq \Delta\theta \leq \frac{L}{2}\right), \\ \Delta\theta - \frac{L}{2} & \left(\Delta\theta > \frac{L}{2}\right). \end{cases} \tag{2}$$

$\Delta\theta$ is joint torsional angle, which means angle difference between motor and load angle. The origin in Fig. 5 is defined as the position where the motor-side gear and the load-side gear are located in the middle of backlash. When $\Delta\theta = \pm\frac{L}{2}$, two gears contact with each other and when $\Delta\theta$ exceeds $\pm\frac{L}{2}$, the output becomes positive or negative.

From the above, the block diagram of a G-IWM model is expressed as the area surrounded by blue dotted line in Fig. 6.

TABLE I
DEFINITION OF PLANT MODEL PARAMETERS

Plant parameters	Definition	Value
Motor inertia	J_m	$0.3\,\mathrm{kgm}^2$
Load inertia	J_l	$1.13\,\mathrm{kgm}^2$
Motor angular velocity	ω_m	-
Load angular velocity	ω_l	-
Joint torsional angular velocity	$\Delta\omega$	-
Joint torsional angle	$\Delta\theta$	-
Motor torque	T_m	-
Joint torque	T_s	-
Joint elasticity	K	$600\,\mathrm{Nm/rad}$
Backlash width	L	$0.0366\,\mathrm{rad}$
Gear ratio	g	4.1739
Half of vehicle mass	M	$650\,\mathrm{kg}$
Half of vehicle normal force	N	$6370\,\mathrm{N}$
Vehicle speed	V	-
Wheel speed	V_ω	-
Driving force	F_d	-
Driving resistance	F_r	-
Tyre radius	r	$0.3\,\mathrm{m}$
Slip ratio	λ	-
Friction coefficient	μ	-

D. Vehice model

A vehicle is driven by driving force, which is generated by friction between wheels and the ground. Driving force is put into wheels as disturbance. This paper focuses on the vehicle starting phase, when gear collision appear severely. Therefore, only longitudinal motion of a vehicle is considered and steering and lateral motion are not taken into consideration. Driving resistance is neglected since it is much smaller than F_d when a vehicle starts. Since our vehicle is driven by two rear IWMs, half-car model is adopted.

The driving force is determined by road friction coefficient and vehicle normal force shown in (3).

$$F_d = \mu N. \tag{3}$$

The definition of parameters is shown in TABLE I. Relationship between λ and friction coefficient μ is expressed by magic formula shown in (4), which is one of famous models for this relation [15] :

$$\mu(\lambda) = D \sin\left(C \tan^{-1} B\left((1-E)\,\lambda + \frac{E}{B}\tan^{-1}(B\lambda)\right)\right). \tag{4}$$

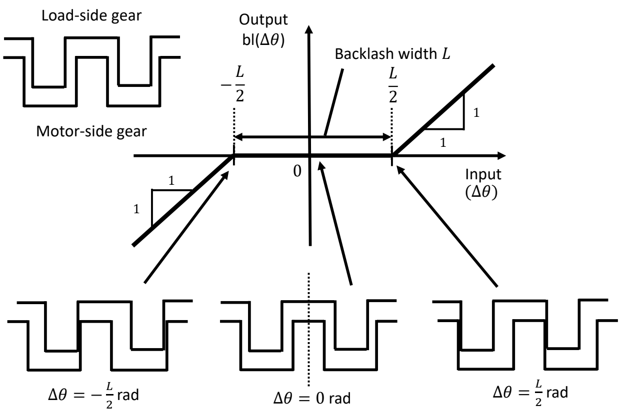

Fig. 5. Deadzone function $\mathrm{bl}(\Delta\theta)$.

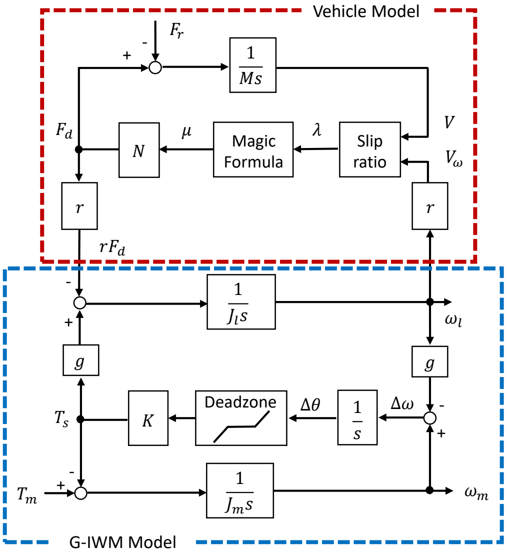

Fig. 6. Block diagram of a G-IWM and a vehicle model.

Slip ratio λ is defined as (5) :

$$\lambda = \frac{r\omega_l - V}{\max(r\omega_l,\, V,\, \epsilon)}. \tag{5}$$

ϵ is the minute value to avoid zero denominator. The equation of longitudinal motion is expressed as (6) :

$$M\dot{V} = F_d - F_r. \tag{6}$$

From the above, the block diagram of a vehicle model is expressed as the area surrounded by red dotted line in Fig. 6.

III. Proposed Method for Gear Collision Reduction

A. Proposed method 1 : Joint torque control using only motor-side encoders

In this method, the vehicle model is used to design controller. Deadzone function in the G-IWM model and magic formula in the vehicle model has nonlinearity and the nonlinear model makes it difficult to design controller. Therefore, the linear model is constructed by assuming that magic formula

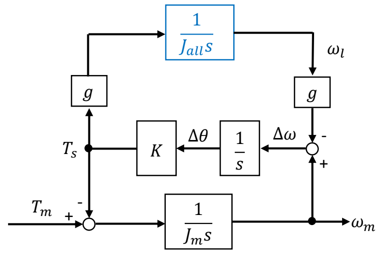

Fig. 7. Block diagram of linear plant model.

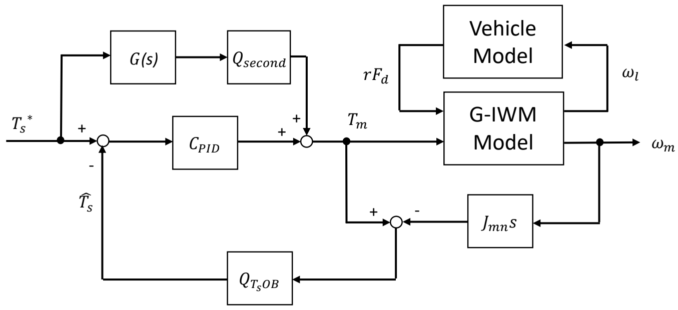

Fig. 8. Block diagram of joint torque control using motor-side encoder.

moves in linear zone. The equations of the load side and the vehicle are expressed as (6) :

$$\lambda = \frac{V_\omega - V}{V_\omega}, \tag{7a}$$

$$\omega_l = \frac{1}{J_l s}(gT_s - rF_d), \tag{7b}$$

$$V = \frac{1}{Ms}F_d, \tag{7c}$$

$$V_\omega = r\omega_l. \tag{7d}$$

By solving these equations, the following (8) can be obtained :

$$\omega_l = \frac{gT_s + Mr^2\omega_l\dot{\lambda}}{\{J_l + Mr^2(1-\lambda)\}s}. \tag{8}$$

To make it easy to design controller, by assuming that the slip ratio is constant λ_n [16], the following (9) can be obtained :

$$\omega_l = \frac{gT_s}{\{J_{ln} + M_n r^2(1-\lambda_n)\}s} \equiv \frac{gT_s}{J_{all}s}. \tag{9}$$

Mass of vehicle is considered to be a part of load-side inertia and total load inertia is expressed as J_{all}. Moreover, nonlinear deadzone function is neglected when designing controller. From the above, the linear plant model shown in Fig. 7 is constructed. Then, feedforward and feedback contoller is designed based on the linear plant model. Its block diagram is shown in Fig. 8. The symbols in the block diagram are shown in TABLE II. The transfer function from motor torque to joint torque is expressed as (10) :

$$\frac{T_s}{T_m} = \frac{KJ_{all}}{J_m J_{all}s^2 + KJ_m g^2 + KJ_{all}}. \tag{10}$$

TABLE II
SYMBOLS IN THE BLOCK DIAGRAM OF JOINT TORQUE CONTROL

Controller parameters	Definition	Value
P controller of motor angular velocity	C_p	-
PI controller of joint torque	C_{PI}	-
PID controller of joint torque	C_{PID}	-
Nominal motor inertia	J_{mn}	$0.3\,\mathrm{kgm}^2$
Nominal load inertia	J_{ln}	$1.13\,\mathrm{kgm}^2$
Joint torque reference	T_s^*	-
Estimated joint torque	$\hat{T}_s$	-
Nominal torsional elasticity	K_n	$600\,\mathrm{Nm/rad}$
Nominal half of vehicle mass	M_n	$650\,\mathrm{kg}$
Nominal slip ratio	λ_n	0.1
Joint torsional angular velocity reference	$\Delta\omega^*$	-
Motor angular velocity reference	${\omega_m}^*$	-
Motor torque reference	${T_m}^*$	-
LPF of joint torque estimator	$Q_{TsOB}(s)$	-
LPF of RFOB	$Q_{RFOB}(s)$	-
LPF to realize motor angular velocity FF control	$Q_{\omega_m FF}(s)$	-
LPF to realize joint torque FF control	$Q_{TsFF}(s)$	-
Second LPF to realize FF control	$Q_{second}(s)$	-

Using the inverse of the transfer function $\frac{T_s}{T_m}$, $G(s)$, and second order low pass filter (LPF) Q_{second} applied to make the transfer function proper, feedforward controller is implemented. The joint torque is estimated by reaction force observer (RFOB) and controlled with PID controller. The PID controller is tuned by the pole placement based on the transfer function $\frac{T_s}{T_m}$. The four poles are set to be same. The gains of PID controller are expressed as equations from (11a) to (11c) :

$$C_{PID} = K_P + \frac{K_I}{s} + K_D \frac{s}{1+\tau_D s}, \tag{11a}$$

$$K_P = \frac{15 J_{mn} J_{all} \omega^2 - 16 K_n J_{mn} g^2 - 16 K_n J_{all}}{16 K_n J_{all}}, \tag{11b}$$

$$K_I = \frac{J_m \omega^3}{4K_n},\ K_D = \frac{81 J_{mn}\omega}{64 K_n},\ \tau_D = \frac{1}{4\omega}. \tag{11c}$$

Here, notice that the proposed method 1 requires vehicle parameters when designing controller.

B. Proposed method 2 : Joint torque control using both motor-side and load-side encoders

The block diagram of the joint torque control using both motor-side and load-side encoders is shown in Fig. 9. It is based on [17] proposed by our research group. The symbols in the block diagram are shown in TABLE II. This proposed method 2 consists of three parts : joint toque feedforward control, joint torque feedback control and motor angular velocity control.

First, the joint torque feedforward controller is introduced. The feedforward controller achieves high bandwidth and improves the performance of reference tracking. The reference of joint torsional angular velocity is generated from the reference of joint torque as follows. From Fig. 6 (12) can be obtained :

$$T_s = K \cdot \mathrm{bl}\left(\frac{\Delta\omega}{s}\right). \tag{12}$$

Then, following (13) can be obtained :

$$\Delta\omega^* = \mathrm{bl}^{-1}\left(\frac{{T_s}^*}{K_n}\right) \cdot s \cdot Q_{T_sFF}(s). \tag{13}$$

The first order low pass filter (LPF) Q_{TsFF} is applied to make the transfer function proper. In order to reduce the maximum motor current, the sigmoid function $\zeta_p(x)$ expressed as (14a) and the novel differentiable inverse deadzone model $\zeta_p(x)$ expressed as (14b) are used as the approximate inverse model of deadzone function :

$$\zeta(x) = K_{sig}\left(\frac{1}{1+e^{-ax}} - \frac{1}{2}\right), \tag{14a}$$

$$\zeta_p(x) = \begin{cases} x + x_1 + \zeta(-x_1) & (x < -x_1), \\ \zeta(x) & (-x_1 \le x \le x_1), \\ x - x_1 + \zeta(x_1) & (x > x_1). \end{cases} \tag{14b}$$

K_{sig} is total gain and a is the gain that determines the similarity to the inverse deadzone model. x_1 is the point where the slope of sigmoid function is 1.

Secondary, the joint torque feedback controller is designed as follows. Feedback control makes it possible to suppress modeling errors and disturbance, such as driving force. The joint torque is estimated by RFOB and controlled with PI controller. The PI controller is tuned by the pole placement to the plant, $T_s = K\frac{1}{s}\Delta\omega$. The first order LPF Q_{TsOB} is applied to make the inverse plant proper. Here, the delay of Q_{TsOB} and Q_{TsFF} has to be considered. Therefore, they are also applied to the joint torque reference.

Finally, ω_m is controlled in the minor loop with feedforward and P feedback controller. By using feedforward controller, high control bandwidth of inner loop is achieved and it improves the performance of the outer joint torque control loop. From Fig. 9, the torsional angular velocity $\Delta\omega$ is obtained as (15) :

$$\Delta\omega = \omega_m - g\omega_l. \tag{15}$$

Then, following (16) can be obtained :

$${\omega_m}^* = \Delta\omega^* + g\omega_l. \tag{16}$$

From (16), the reference of ω_m is generated from the reference of $\Delta\omega$ and ω_l, which can be obtained with load-side encoders. Then, motor torque is compensated by joint torque estimated by RFOB. The first order low pass filter (LPF) Q_{RFOB} is applied to make the transfer function proper. Feedforward controller is implemented by the inverse motor model based on the assumption that joint torque is decoupled from the motor-side by RFOB. The first order low pass filter (LPF) $Q_{\omega_m FF}$ is applied to make the transfer function proper. Motor angular velocity is controlled with P controller. P controller is tuned by considering the stable margin. The control cycle of motor current is so short that motor torque reference equals motor torque input.

Here, notice that load-side encoders make it possible to control joint torque without vehicle parameters and to make inner motor angular velocity loop, which improves the performance of the outer joint torque control loop.

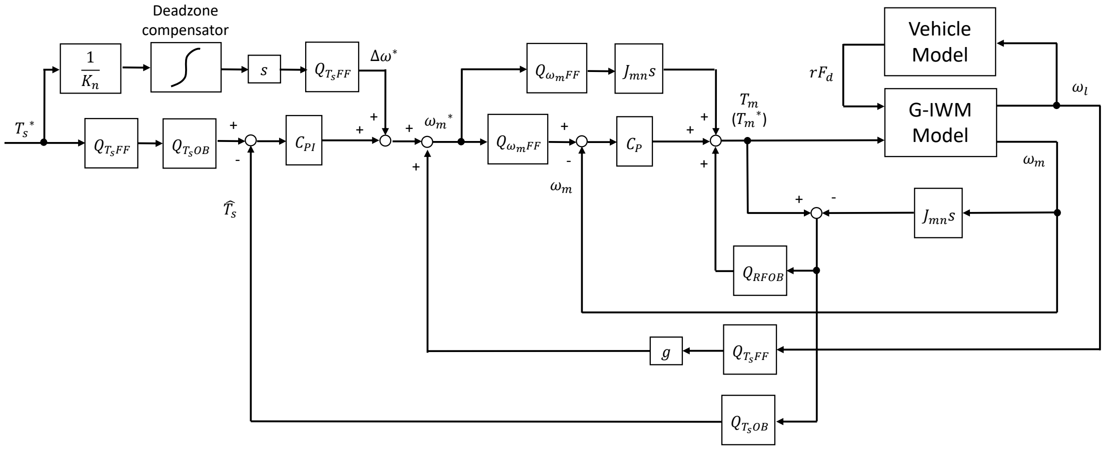

Fig. 9. Block diagram of joint torque control using both motor-side and load-side encoders [17].

IV. Simulations

A. Simulation situations

The parameters used in the simulations are shown in TABLE I and II. $B = 11.43$, $C = 1.314$, $D = 1$, $E = -0.225$ is adopted in (4), $\epsilon = 1e - 5$ is introduced in (5) to avoid zero denominator and $K_{sig} = 0.04$, $a = 5000$ is selected in (14a). Cutoff frequency of LPF is $50\,\mathrm{Hz}$. Gain of P controller is 10 and poles of PI and PID controller is $7\,\mathrm{Hz}$. The joint torque reference is set to be ramp function which increases to $64\,\mathrm{Nm}$ in $10\,\mathrm{s}$ and it supposes gradual acceleration. The initial position of gears is determined to make joint torsional angle equal to $-\frac{L}{2}$, where gear collision appear most severely.

B. Simulation results

Fig. 10(a) shows the motor torque. The motor torque of the proposed method 2 is larger than that of the proposed method 1 for $0.2\,\mathrm{s}$ after starting. Therefore, the proposed method 2 enables gears to mesh more quickly. The motor torque of the two methods are negative just after gear collision to reduce the impact. Fig. 10(b) shows the joint torque. The joint torque of two methods are zero just after starting because gears do not mesh with each other. Gears mesh more quickly in the proposed method 2 as indicated in Fig. 10(a). The maximum value of joint torque after collision of the proposed method 2 is smaller. This implies that the impact of gear collision is reduced by using load-side encoders. In the proposed method 2, the joint torque follows the reference more quickly without a steady-state error and does not vibrate. On the other hand, In the proposed method 1, it takes about $0.5\,\mathrm{s}$ to follow the reference and a steady-state error exists because of the shortage of integrators. Fig. 10(c) shows the joint torsional angle. Two gears do not mesh in the area surrounded by two black dotted lines. In the proposed method 2, with load-side encoders, gears mesh more quickly and the impact of collision is reduced.

V. Experiments

A. Experimental situations

The nominal value and P and PI controller gains used in the experiments are same as those in the simulations. The cutoff frequency of LPF, the total gain of sigmoid function K_{sig} and the similarity gain a are experimentally tuned. In the beginning, minute minus motor torque is inputted and the motor side and the load side are meshed with each other. After that, the proposed method 2 is implemented and the experimental vehicle starts on the flat asphalt road shown in Fig. 2.

B. Experimental results

Fig. 11(a) shows the motor torque of the proposed method 2. The motor torque corresponds to Fig. 10(a). Fig. 11(b) shows the reference of the joint torque and the estimated joint torque of the proposed method 2. The estimated joint torque follows the reference. On the other hand, the noise of the motor speed generates an error. Fig. 11(c) shows the joint torsional angle of the proposed method 2. It corresponds to Fig. 10(c). Gears mesh quickly and the vibration and the impact of collision is suppressed.

VI. Conclusion

The vibration and noise caused by gear collision of G-IWMs deteriorate the ride comfort and a solution is required. In previous study, our research group proposed to apply joint torque control using load-side encoders for two-inertia system and the effectiveness is validated. However, in point of space and costs, mounting load-side encoders is not desirable and the effect of mounting them should be investigated. In this paper, the joint torque control using both motor-side and load-side encoders is compared with the joint torque control using only motor-side encoders. Simulations and experiments reveal that using load-side encoders makes it easy to design controller, to control joint torque quickly and to reduce the impact of collision.

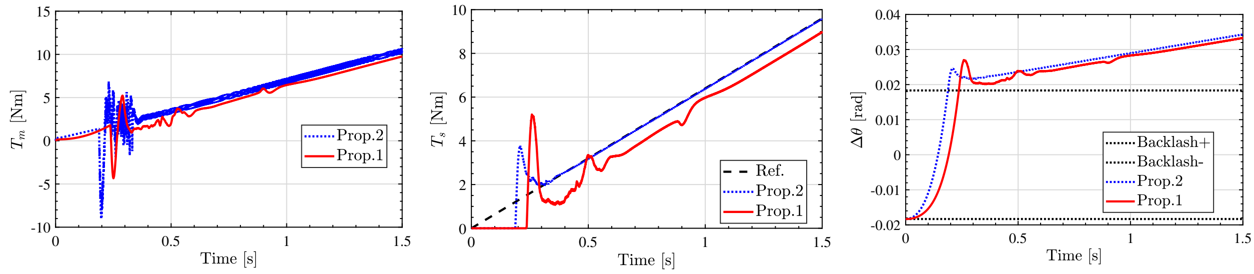

(a) Motor torque T_m.

(b) Joint torque T_s.

(c) Joint torsional angle $\Delta\theta$.

Fig. 10. Simulation results.

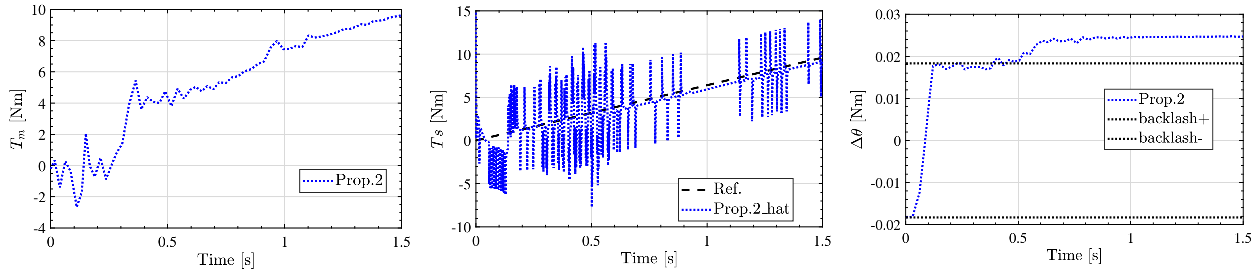

(a) Motor torque T_m.

(b) Joint torque T_s.

(c) Joint torsional angle $\Delta\theta$.

Fig. 11. Experimental results.

ACKNOWLEDGMENT

This work was partly supported by JSPS KAKENHI Grant Number 18H03768. Finally, the authors would like to express their deepest appreciation to Nikon Corporation, Toyo Denki Seizo K.K and NSK for providing the encoders, the inverter, the motor, and the gear used in the experiments.

REFERENCES

[1] V.-D. Doan, H. Fujimoto, T. Koseki, T. Yasuda, H. Kishi, and T. Fujita, "Simultaneous Optimization of Speed Profile and Allocation of Wireless Power Transfer System for Autonomous Driving Electric Vehicles," *IEEJ Journal of Industry Applications*, vol. 7, no. 2, pp. 189–201, 2018.

[2] Y. Hori, "Future vehicle driven by electricity and control - Research on four-wheel-motored "UOT Electric March II"," *IEEE Transactions on Industrial Electronics*, vol. 51, no. 5, pp. 954–962, 2004.

[3] S. Hara, K. Miyata, K. Suzuki, and M. Tsukamoto, "Effectiveness Evaluation of Updating Final-State Control for Automated Guided Vehicles Motion Control with Collision Avoidance Problems," *IEEJ Journal of Industry Applications*, vol. 7, no. 4, pp. 358–368, 2018.

[4] S. Murata, "Innovation by in-wheel-motor drive unit," *Vehicle System Dynamics*, vol. 50, no. 6, pp. 807–830, 2012.

[5] W.-P. Chiang, D. Yin, M. Omae, and H. Shimizu, "Integrated Slip-Based Torque Control of Antilock Braking System for In-Wheel Motor Electric Vehicle," *IEEJ Journal of Industry Applications*, vol. 3, no. 4, pp. 318–327, 2014.

[6] T. Makino, "Recent technology trend of in-wheel motor system for automotive vehicle," *Toraibarojisuto/Journal of Japanese Society of Tribologists*, vol. 58, no. 5, pp. 310–316, 2013.

[7] K. Yuki, T. Murakami, and K. Ohnishi, "Vibration control of 2 mass resonant system by resonance ratio control," *Proceedings of IECON '93 - 19th Annual Conference of IEEE Industrial Electronics*, pp. 2009–2014, 1993.

[8] M. Nordin and P. O. Gutman, "Controlling mechanical systems with backlash - A survey," *Automatica*, vol. 38, no. 10, pp. 1633–1649, 2002.

[9] J. Motosugi, O. Sho, S. Akira, and F. Kengo, "Motor Control Technologies for Improving the Driving Performance of Electric Vehicles," *EVS31&EVTeC*, 2018.

[10] S. Wakui, T. Enmei, H. Fujimoto, and Y. Hori, "Gear Collision Reduction of In-wheel-motor by Joint Torque Control Using Load-side High-resolution Encoder," *IEEE International Conference on Mechatronics*, pp. 550–555, 2019.

[11] M. Ruderman and M. Iwasaki, "Sensorless Torsion Control of Elastic-Joint Robots with Hysteresis and Friction," *IEEE Transactions on Industrial Electronics*, vol. 63, no. 3, pp. 1889–1899, 2016.

[12] P. Weiss, P. Zenker, and E. Maehle, "Feed-forward friction and inertia compensation for improving backdrivability of motors," *2012 12th International Conference on Control, Automation, Robotics and Vision, ICARCV 2012*, vol. 2012, no. December, pp. 288–293, 2012.

[13] C. Mitsantisuk, M. Nandayapa, K. Ohishi, and S. Katsura, "Design for Sensorless Force Control of Flexible Robot by Using Resonance Ratio Control Based on Coefficient Diagram Method," *Automatika Journal for Control, Measurement, Electronics, Computing and Communications*, vol. 54, no. 1, 2013.

[14] S. Oh and K. Kong, "High-Precision Robust Force Control of a Series Elastic Actuator," *IEEE/ASME Transactions on Mechatronics*, vol. 22, no. 1, pp. 71–80, 2017.

[15] H. B. Pacejka and E. Bakker, "The Magic Formula Tyre Model," *Vehicle System Dynamics : International Journal of Vehicle Mechanics and Mobility*, vol. 21, no. 1, pp. 1–18, 1922.

[16] K. Fujii and H. Fujimoto, "Traction control based on slip ratio estimation without detecting vehicle speed for electric vehicle," *Fourth Power Conversion Conference-NAGOYA, PCC-NAGOYA 2007 - Conference Proceedings*, pp. 688–693, 2007.

[17] S. Yamada and H. Fujimoto, "Precise Joint Torque Control Method for Two-inertia System with Backlash Using Load-side Encoder," *IEEJ Journal of Industry Applications*, vol. 8, no. 1, pp. 75–83, 2018.